Disc Fluttering in Stratified Flows

Try Lam, Lionel Vincent and Eva Kanso†

Department of Aerospace and Mechanical Engineering, University of Southern California, Los Angeles, CA 90089, USA

(Received xx; revised xx; accepted xx)

Key words: fluttering motion, stratified flow, free-falling motion [placeholder for entry; remove before submitting]

1. Introduction

The motion of a descending disc in a fluid is rich in dynamics with complex interaction between the fluid and solid. Such un-steady free falling behaviors has attracted the attention of scientists as early as 1853 with Maxwell as he observed a rectangular slip of paper falling through the air (Maxwell 1990). Throughout the years, the falling patterns and associated phase space has been progressively refined for both numerical and experimental studies, and found that for small thickness-to-width ratio the falling patterns depend on the Reynolds number, Re, and the dimensionless moment of inertia, I^*.

Notably, Willmarth *et al.* (1964) constructed a phase diagram by experimentally dropping disks with various thickness-to-width ratio. They were able to define a clear boundary in the phase space between steady and unsteady (fluttering and tumbling) oscillating motion. For $Re < 100$, viscous forces dominates and a disc motion released with near zero initial conditions will descend steadily with small to no libration independent of I^*. For larger values of Re, when inertial forces plays a more dominate role, other three descent modes can be observed for difference ranges of I^*, as noted in Field *et al.* (1997). Stringham *et al.* (1969) perform similar experiments with spheres, cylinders, and disks and computed drag coefficients for a wide range of Reynolds numbers. Field *et al.* (1997) also experimented with varying initial release angles (disk's normal to the vertical) and found that the final angle is a function of the initial angle. See Ern *et al.* (2012) for a comprehensive review of both experimental and computational techniques of free-falling bodies in fluids. In general, the descent motion falls into four main types: steady, fluttering, tumbling, or chaotic depending on Re and I^*, where $Re = Ud/\nu$, and the dimensionless moment of inertia, $I^* = I/\rho_f d^5 = \pi\rho t/64\rho_f d$, where U is the mean vertical velocity ($U = h/T$), h is the descent height, T is the total time of the descent, ν is kinematic viscosity of the fluid, d is diameter of the disc, t is the disc's thickness, ρ is the density of the disc, ρ_f is the density of the fluid.

Recently, Auguste *et al.* (2013) numerically explored similar falling motion of discs with parameter space in I^* and Archimedes number $Ar = \sqrt{3/32}U_g d/\nu$, which is a modified Reynolds number with gravitational speed $U_g = \sqrt{2|\rho/\rho_f - 1|gh}$. In their study, they explored $Re < 300$ (or approximately $Ar < 110$), and defined additional non-planar sub-regimes they called hula-hoop (gyrating while fluttering) and helical autorotation

† Email address for correspondence: kanso@usc.edu

(tumbling with plane rotation). The hula-hoop behavior was also observed in Heisinger *et al.* (2014). This zigzag or fluttering motion was also experimentally investigate by Zhong *et al.* (2013) where they used dye visualization and particle image velocimetry (PIV) to understand the flow structure of fluttering motion for different disc thickness to diameter ratios. Lee *et al.* (2013) expanded the experiment by looking at transitions from two-dimensional fluttering to spiral motions, and noted a critical Reynolds number where the transition occurs. Lee *et al.* (2013) also looked at different initial release angles and the affect on the fluttering trajectories.

Numerical investigations were also conducted by Jin & Xu (2008), Pesavento & Wang (2004), Andersen *et al.* (2005*a*), Andersen *et al.* (2005*b*), and Chrust *et al.* (2013) for thin discs and cards. Jin & Xu (2008) developed a moving mesh method for Navier-Stokes equations and had good agreements between expiermental and computational trajectories, and clarified some discrepancies noted in Andersen *et al.* (2005*b*), who along with Andersen *et al.* (2005*a*) and Andersen *et al.* (2005*b*) studied the free falling dynamics in a quasi-steady force model in the body frame. Similar to Auguste *et al.* (2013), Chrust *et al.* (2013) numerically studied the dynamics of free falling disc, but parameterize the phase space using the non-dimensionalized mass $m^* = m/\rho_f d^3$ and the Galileo number $G = \sqrt{|m^* - (V/d^3)|gd^3}/\nu$, where V is the volume of the body. The Archimedes number is related to the Galileo number by $Ar = \sqrt{3/4\pi}G$. Recently, Kuznetsov (2015) numerically study the regular and chaotic bahaviors of falling plates using the quasi-steady models introduced by Tanabe & Kaneko (1994), Belmonte *et al.* (1998), Pesavento & Wang (2004), and found two-dimensional descent motion to be rich in dynamics with nonlinear characteristics such as fixed points, limit cycles, attractors, and bifurcations.

Recent experimental studies by Heisinger *et al.* (2014), found probability density functions (*pdf*) associated with the landing distribution for each of the four falling modes. They found that the center is one of the least likely landing site for non-steady descents, characterized by dips in the *pdf* around the center. For tumbling descent, the *pdf* forms a ring structure about the center, while for chaotic descents, the *pdf* distribution is much more widely distributed. Vincent *et al.* (2016) later investigate the falling behaviors of annular discs in the same Re and I^* space, and found the central hole in the disc to be a stabilizer of the descent motion as the inner edge forms an counter-rotating vortex ring to that of the outer edge.

In the previous examples, the fluid flow were homogenous. In this paper, we experimentally investigate the motion of fluttering discs in vertically stratified salt-water fluid and compare the motion to that of homogenous water. The descent motion trajectory and orientation are reconstructed for the free-fall fluttering disc. The final landing location for multiple drops are also recorded to compute the landing distribution. For a vertically stratified fluid the tank will have a linear fluid density gradient with higher density at the bottom and lower density on top. The summary of the overall process and experiment is illustrated in figure 1.

Such vertical density variations exist in nature and can be seen in lakes, oceans, and the atmosphere. This is especially notable in isolated environments such as pores and fractures where mixing is negligible (MacIntyre *et al.* 2014), where they noted intense biological activity and accumulation of particles and organisms associated with vertical fluid density variations. In addition, Ivey (2004) reported that smallest particle length scale that can be affected by salt-stratification is less than 1 mm based on the Rayleigh number Ra.

As mentioned above, motion in homogenous fluid can be parameterized by the Reynolds number Re, and non-dimensional moment of inertia I. For the case of

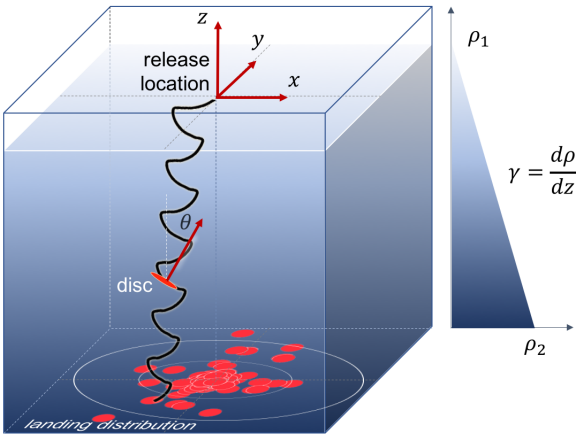

FIGURE 1. (Colour online) Schematic of the tank setup with the coordinate system centered at the initial release location. The descent motion is reconstructed for the free-fall fluttering disc as shown, where the inclination angle, θ, is the angle between the XY-plane and the direction normal to the face of the disc. The final landing location for multiple drops are also recorded to compute the landing distribution. For a vertically stratified fluid the tank will have a linear fluid density gradient, $\gamma = d\rho/dz$, with higher density at the bottom of the tank, ρ_2, and lower density at the top, ρ_1.

stratified fluid, buoyancy becomes important, and can be described in terms of Froude number $Fr = U/Nd$, which represents the buoyancy force, where $N = (-\gamma g/\rho_0)^{1/2}$ is the Brunt-Väisälä (stratification) frequency, or the natural frequency of oscillaiton of a vertically displaced fluid parcel in the stratified fluid, ρ_0 is a reference density, and $\gamma = d\rho/dz < 0$ is the density gradient of the fluid (negative for increasing density with increasing depth). The Froude number tells us about the stability and strength of the stratification. For strong stable stratificaiton, the Froude number is a small real number. The Reynolds number Re and Froude number Fr can be combined and expressed in terms of the viscous Richardson number $Ri = Re/Fr^2$.

2. Methods

To investigate how the presence of stratified flow influence the trajectory descent motion a disc and fluid system is selected, such that, the descent mode does not change after stratification, i.e., the fluttering motion of a disc observed in homogenous water will persist even after the background fluid is now linearly stratified with salt-water. Although, a transition in the descent mode would be of interests, our initial investigation is to understand the quantitative differences of a disc in free-falling fluttering descent when the fluid is stratified and no longer homogenous.

Due to practical experimental limitations, such as safety and cost, we elected to use salt-water for the stratification process. A two-tank (or double-tank) method is used to generate a stable linear density profile in the main or test tank. This method was proposed by Fortuin (1960) and Oster (1965), where a forced-drained approach applying mechanical pumps to control the fluid flow was used. A summary of the setup and stratification process can be reviewed in Hill (2002). Here we use a free-drained approach, which rely on gravity and not pumps, to produce the linear vertical stratification. To produce a top-filled stable vertical stratification ($\gamma = d\rho/dz < 0$) with the higher density

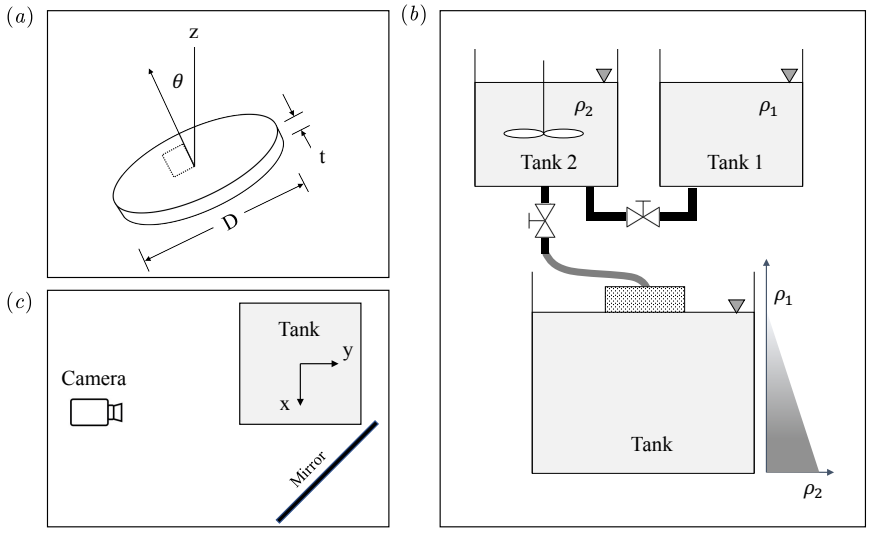

FIGURE 2. (*a*) Disc schematic (diameter d and thickness t) where θ is the angle between the vertical z direction and the disc normal direction. (*b*) Two-tank experimental free-drained setup used to generate a stable linear density profile in the tank. Tank 1 and Tank 2 are equal in volume filled with fluid of different densities. During the stratification process, the lower density fluid (ρ_1) flows to the higher density (ρ_2) tank where it is mixed prior to flowing to the main experimental tank. A sponge and floater are used to ensure that the fluid is evenly distributed and remains top filled. (*c*) Top view of the experimental tank and camera setup. A mirror is placed and aligned to obtain the orthogonal side view of the tank needed for the image processing and reconstruction of the disc's trajectory and orientation.

at the bottom and the lower density solution at the top of the tank, two tanks of equal sizes (approximate 1/2 of the main tank) with different density is required. In our case the fluid lower density fluid is water ($\rho_1 \approx 1000\ kg/m^3$) and the higher density is salt-water solution ρ_2. During the tank filling process, the lower density fluid (ρ_1) flows to the higher density (ρ_2) tank where it is mixed prior to filling the main experimental tank. A sponge and floater are used to ensure that the fluid is evenly distributed by minimizing mixing and remains top filled. A schematic showing the setup is shown in figure 2b.

To investigate the fluttering motion, an acrylic disc ($\rho = 1143.7\ kg/m^3$) with dimensions $d = 2.54\ cm$ and $t = 2\ mm$ (see figure 2a) are released in water was selected for the baseline case. In the (Re, I^*) space, this place the motion in the fluttering mode regime with a dimensionless moment of inertia $I^* = 0.0035$ and Reynolds number of $Re = 1640$. The average speed U is not known *a priori* and is found by experimentally dropping the disc and recording the time it takes to descend the length of the tank.

The investigation tank is a cubic acrylic container, 0.61 m on each side (≈ 60 gallons), see figures 1 and 2b. In the experiments, the discs were released with near zero initial conditions just below the surface of the fluid using an electromagnetic release mechanism. To determine the uncertainty inherent in the release mechanism, a steel disc in air is released using the mechanism TBD times. The standard deviation of the steel disc descent was within $TBD\%$ of the vertical drop distance. [TBD: NEED TO TEST THIS]

For the landing distribution, the location of the disc at the bottom of the tank is recorded with a top mounted camera. To prevent the disc from sliding while it lands a grid mesh is added to to the bottom of the tank. For the reconstruction of the descent

Case	$N(rad/sec)$	σ_1/h	σ_2/h	r_m/h	r_{var}/h	90% *cdf*
Water	0	0.055	0.036	0.060	0.002	$r/h = 0.11$
Stratified	1.69	0.097	0.078	0.084	0.011	$r/h = 0.20$

TABLE 1. Distribution parameters of the final landing distribution. σ_1 and σ_2 are the standard deviations along the major and minor axes from figure 3. r_m and r_{var} are the mean and variance of the radial distribution normalize by the descent height h, and *cdf* is the cumulative distribution function as shown in figure 4.

trajectory and orientation, the fluttering descents were recorded using a high resolution digital video camera (Point Grey Grasshopper3) set to a moderate frame rate > 50 fps. The camera and tank setup is shown in figure 2c. To obtain the corresponding side view of the disc's descent a mirror is used instead of multiple cameras. Proper calibration is required to adjust for the mirrored view. The position and orientation are obtained directly from the reconstructed trajectory after high frequency noise are removed. The velocity and orientation rates were obtained using finite differencing. The experimental setup and procedure, including the image processing algorithm for the trajectory and orientation reconstructions, are similar to those of Heisinger *et al.* (2014) and Vincent *et al.* (2016).

3. Results

To test the influence stratification has on the disc's trajectory in the fluttering regime we use pure water as our baseline for the disc and tank described in §2. Drops are made in water and near identical drops are made in the stratified flow. We seek to observe (1) the affect stratification has on the landing distribution, and (2) the affect stratification has on the disc's trajectory and orientation.

3.1. *Landing Distribution*

Repeating the experiment done by Heisinger *et al.* (2014), we made multiple repeated drops (500) in homogenous water to obtain our baseline for the fluttering case. The resulting landing distribution for the drops in water, expressed as histogram of probability per unit bin, is shown in figure 3a, and the radial distribution is shown in figure 4a. Our results are similar to those by Heisinger *et al.* (2014), where a dip in the radial histogram near the origin and a tight radial distribution ($\sigma < 10\%$ descent height) are observed.

To observe the influence stratification has on the radial distribution we repeat the (500) drops in stratified flow with $N = 1.69$ rad/sec (density gradient $\gamma = -290\ kg/m^4$). Figure 3b shows the distribution of the landing location for stratified flow case; when compared to figure 3a, we note a larger radial dispersion. This is more evident in figure 4a, which shows the histogram of the radial distributions for both water and stratified flow. Observing the cumulative distribution function (*cdf*) in figure 4b, we observe that two curves deviate quickly after $r/h > 0.05$. At 0.11 r/h 90% of the drops in water are contained. For the stratified case, the 90% cumulation is reached at 0.20 r/h. A summary of the distribution parameters are listed in table 1.

3.2. *Trajectory Reconstruction*

To investigate further the affect stratification has on descent fluttering motion, trajectories are reconstructed in water and stratified flow, at $N = 1.06$ rad/sec and $N = 1.69$ rad/sec, with focus on the later. The discs are released with near zero initial conditions

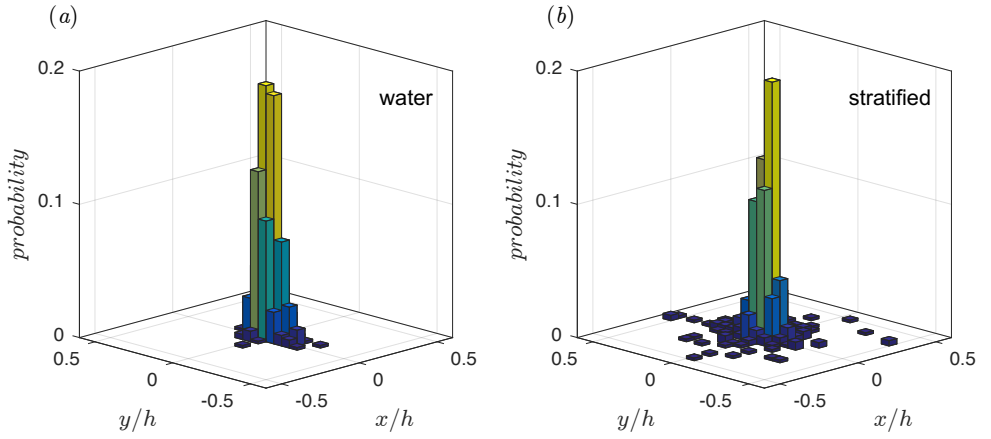

FIGURE 3. (Colour online) Distribution of the final landing location, expressed in probability per bin, for 500 free-fall fluttering discs in (a) water and (b) stratified flow, where x and y are normalized by the depth of the fluid, h. The vertically stratified fluid has a density gradient $\gamma = -290\ kg/m^4$ and stratification frequency $N = 1.69\ rad/sec$. Disc are initially released at $(x, y) = (0,0)$. Assuming normal distribution profiles, the ratio of the mean standard deviations of the final landing distribution for descents in stratified flow to that of water, $< \sigma >_{strat} / < \sigma >_w = 1.92$.

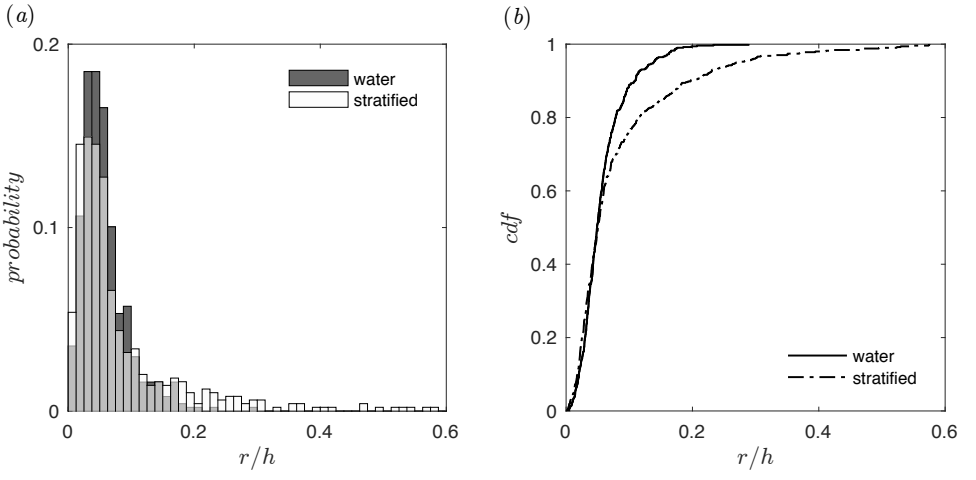

FIGURE 4. (a) Histogram of the range distribution at their final landing location, expressed in probability per bin, for 500 free-fall fluttering discs in both water and stratified flow, where r is normalized by the depth of the fluid, h. For the stratified flow, it has density gradient $\gamma = -290\ kg/m^4$ and stratification frequency $N = 1.69\ rad/sec$. (b) The cumulative distribution function (*cdf*) is plotted as a function of normalized range r/h for both the descents in water and stratified flow. Assuming a lognormal probability density function, the variance for the descents are $\nu_w = 0.002$ for water and $\nu_{strat} = 0.011$ for stratified flow, or $\sqrt{\nu_{strat}/\nu_w} = 2.35$. The differences in the mean is $m_w = 0.06$ for water and $m_{strat} = 0.084$ for stratified flow, or $m_{strat}/m_w = 1.4$. From the *cdf* plot in (b) we note that 90% of the cases are reached at $r/h = 0.11$ for water and $r/h = 0.20$ for stratified flow.

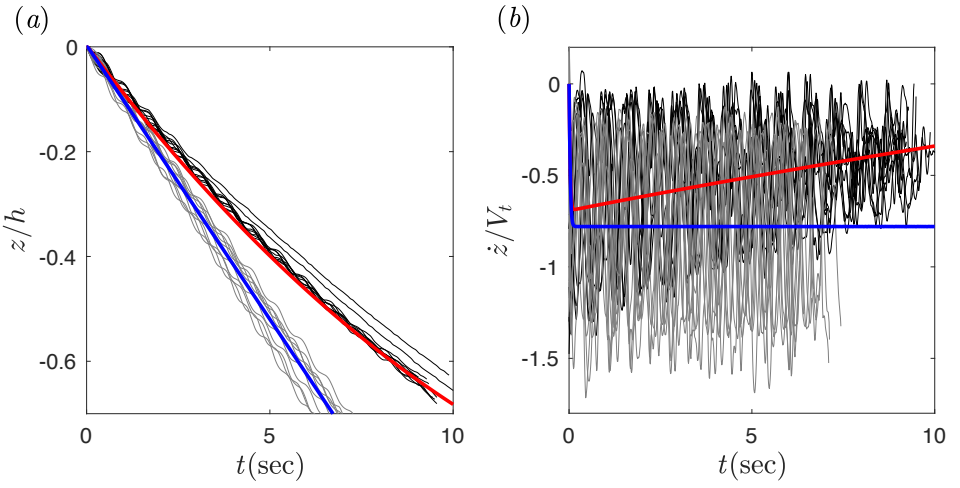

FIGURE 5. (Colour online) (*a*) Descent depth z and (*b*) descent velocity $\dot{z}$ as a function of time for free fall fluttering discs in water (−) and $N = 1.69$ rad/sec stratified flow (−), where z is normalized by the depth of the fluid, h and $\dot{z}$ is normalized by the terminal speed in water V_t. Curve fits to the mean respective cases using (3.2.1) are overlaid in bold lines where $C_D = 1.44$ for water descents (blue curve) and $C_D = 1.83$ for stratified flow (red).

top center of the tank, with the x-axis along the front of the tank (left-to-right), y-axis along the depth of the tank, and z-axis along the height of the tank centered at the initial drop location, as illustrated in figure 1. Coin descents are recorded and processed as described in §2 for reconstructing the position and orientation information.

3.2.1. *Effect of Stratification on Translational Motion*

A pronounced result of stratification is the affect it has on the vertical descent motion, z. Figure 5 shows the vertical descent motion z and $\dot{z}$, where z is normalized by the depth of the fluid h, and $\dot{z}$ is normalized by the terminal speed in water, $V_t = 7.16$ cm/sec. Here we note the difference in the descent time. In the pure water fluid, the average disc descent times were approximately 6.5 seconds, while the cases in stratified fluid were nearing ten seconds to descend. In addition to the descent duration, the slope of z as a function of time is no longer linear for the cases in stratified flow, indicating a deceleration in speed as it descends. This deceleration is clearly seen in figure 5b and in figure 6a, where the average speed of the descents are plotted as a function of time. To focus only of the fully developed fluttering descent motion, the first few cycles of the transient behavior were removed in figure 6a. Looking at the average descent speed, the descents in water approaches 5.59 ± 0.33 cm/sec and remain steady with a negative slope. For the descents in stratified fluid (−) the average descent speed approaches 3.89 ± 0.15 cm/sec. An upward (positive z) slope or acceleration of 0.85 ± 0.16 mm/sec^2 exist. A summary comparing the reconstructed results between descents in water and descents in stratified flow are shown in figure 8.

It is noted, that the vertical descent motion in figure 5 follows closely to the dynamics of a simple descending particle of the form

$$\ddot{z} = -g + \frac{1}{m}\rho_f(z)\,Vg + \frac{1}{2m}\rho_f(z)\,|\dot{z}|^2 C_D A \tag{3.1}$$

where gravity constant $g = 9.806$ m/s^2, V is the volume of the disc, C_D is the drag

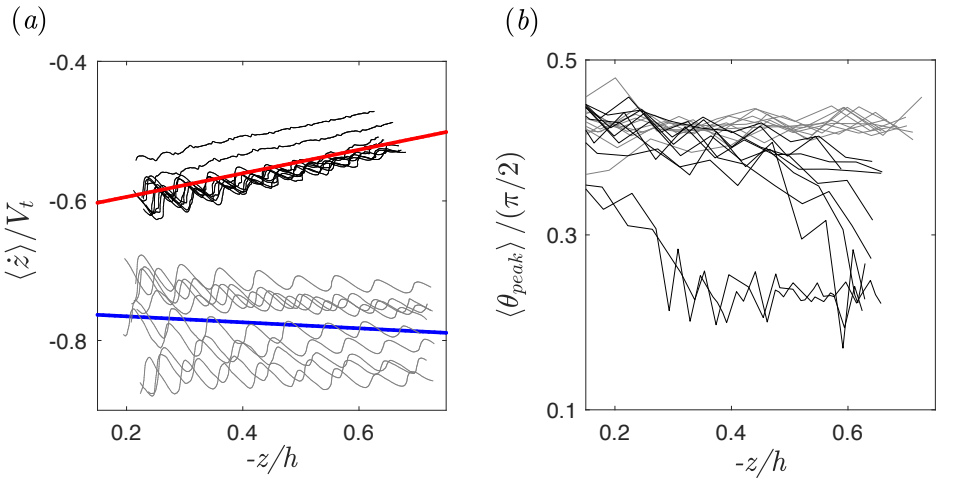

FIGURE 6. (Colour online) Average (a) vertical velocity normalized by the terminal speed V_t in water, and (b) peak inclination (maximum inclination angle at the inflection point where the angular rate is near zero) as a function of depth ($-z$), where $-z$ is normalized by the depth of the fluid, h. Cases in water (−) and $N = 1.69$ rad/sec stratified fluid (−). Linear curve fit to the mean cases are overlaid in bold blue for water descents and bold red for cases stratified flow, where the slope is -0.043 for water and 0.169 for stratified flow.

coefficient, area $A = \pi d^2/4$, m is the mass, $\rho_f(z) = \rho_0 + \gamma z$, and density gradient $\gamma = d\rho/dz$. The z and $\dot{z}$ state from the dynamical model is overlaid in figure 5 for $C_D = 1.44$ for water descents and $C_D = 1.83$ for stratified flow, where the value of C_D is selected to best fit to the average reconstructed z state. In both figures we note acceptable agreements for predicting the vertical motion.

We also note that the C_D for stratified flow is larger than that of water, $C_D^{Strat}/C_D^{Water} = 1.27$. This increase or enhanced drag has also been observed by Torres *et al.* (2000) and Yick *et al.* (2009) for vertical motion of spheres in stratified flow, and found correlations between C_D and the Froude number Fr.

3.2.2. *Effect of Stratification on Orientational Motion*

As the discs descends in the fluttering mode, the inclination (angle between the norm vector of the coin and z-axis) will oscillate between extremas as it cycles from maximum inclination to zero inclination to minimal inclination and back to zero inclination. This inclination frequency has been observed to be 1.63 Hz for the average ten reconstructed descent cases in water and 1.44 Hz for the descents in stratified flow. In figure 6b the peak inclination angle (the maximum angle between the norm vector of the coin and z-axis at the inflection point where the angular rate is near zero) is plotted for ten descents in water (−) and the ten descents in stratified fluid (−).

From figure 6b, a notable decrease in the peak inclination is shown for the stratified cases 32.1 ± 5.7 deg versus 38.2 ± 0.5 deg in water, and the peak inclination descent rate for the stratified case is approximately -1.3 ± 0.7 deg/sec as oppose to that of water water which is approximately 0.14 ± 0.26 deg/sec. We believe this decease in inclination rate in the stratified fluid is due to a small restoring torque that exist between the center of gravity and the center of buoyancy. When the inclination angle is non-zero the side of the coin closer to the bottom of the tank will experience higher buoyancy force due to its higher density, thus, causing a torque in the direction which minimizes the inclination

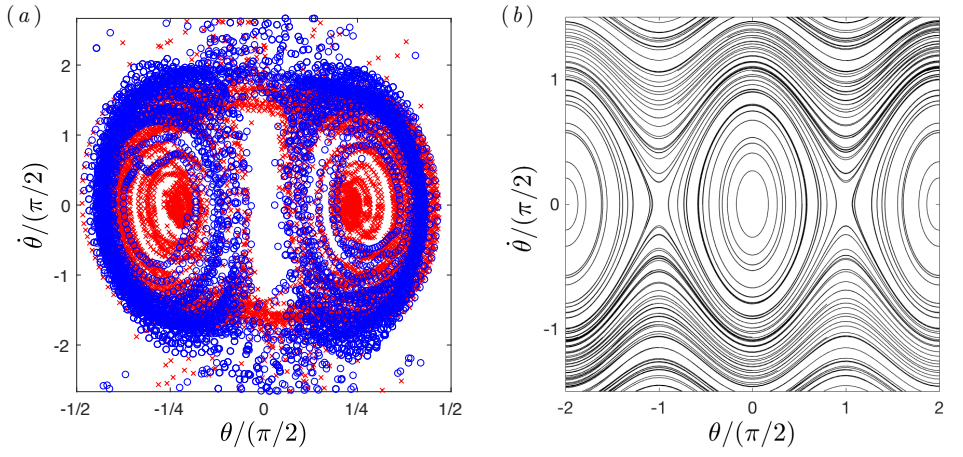

FIGURE 7. (Colour online) (*a*) θ-$\dot{\theta}$ phase plot for fluttering descents in water (○) and $N = 1.69$ rad/sec stratified fluid (*x*). (*b*) θ-$\dot{\theta}$ phase plot due to analytical buoyancy driven angular oscillation.

angle. From a hydrostatic model the restoring acceleration is found by computing the buoyancy offset due to the stratification by integrating the buoyancy element over the disc's volume, and is found to be

$$\ddot{\theta}_B = -\frac{\rho_0}{2\rho} N^2 sin\,(2\theta) \tag{3.2}$$

where ρ_0 is the reference density of the fluid, ρ is the density of the disc, N is the Brunt-Väisälä freqency, and θ is the inclination or nutation angle. For $N = 1.69$ rad/sec, equation 3.2.2 gives a maximum radial restoring acceleration of 142.9 deg/sec^2 at ± 45 deg and zero at 0 deg and at ± 90 deg. For the derivation of the above equation, see §A.

From the Brunt-Väisälä frequency N, we understand how stratification affects vertical translational motion, as it gives the angular frequency of the buoyancy driven oscillation, but from 3.2.2 we have a key relationship on how stratification effects orientational dynamics. Equation 3.2.2 provides a non-linear relation with θ, that is similar to the motion of pendulum (see θ and $\dot{\theta}$ phase space for 3.2.2 in figure 7b). If a dissipative angular acceleration term is added to the equations of motion (of the form $-k\dot{\theta}$, where k is some constant), this will cause both θ and $\dot{\theta}$ to approach zero as time progress.

However, from experimental data (figure 7a), we do not always observe such behavior for fluttering descents with or without stratification. Instead it appears that for some csaes, the librating region occurs away from $\theta = 0$ in pairs, yet still bounded to $\theta_{max} \approx \pm 45$ deg. The result is consistent with our understanding of disc dynamics for non-steady descents, where a disc released with zero initial inclination would begin to rotate and the disc would eventually either flutter, tumble, or a chaotic combination of fluttering and tumbling. Furthermore, these librating regions around the $\approx \pm 20$ deg fixed points, corresponds to hula-hoop descents (Auguste *et al.* 2013), where the inclination angle never goes to zero, but precess with a near constant angle. Note that, although the inclination angle is taken always to be positive, by definition, in selected analysis it is useful to define a moving plane to view orientation changes comparable to experiments and computations done in two dimensions, as with figure 7a.

Reconstructed results between descents in water and descents in stratified flows are

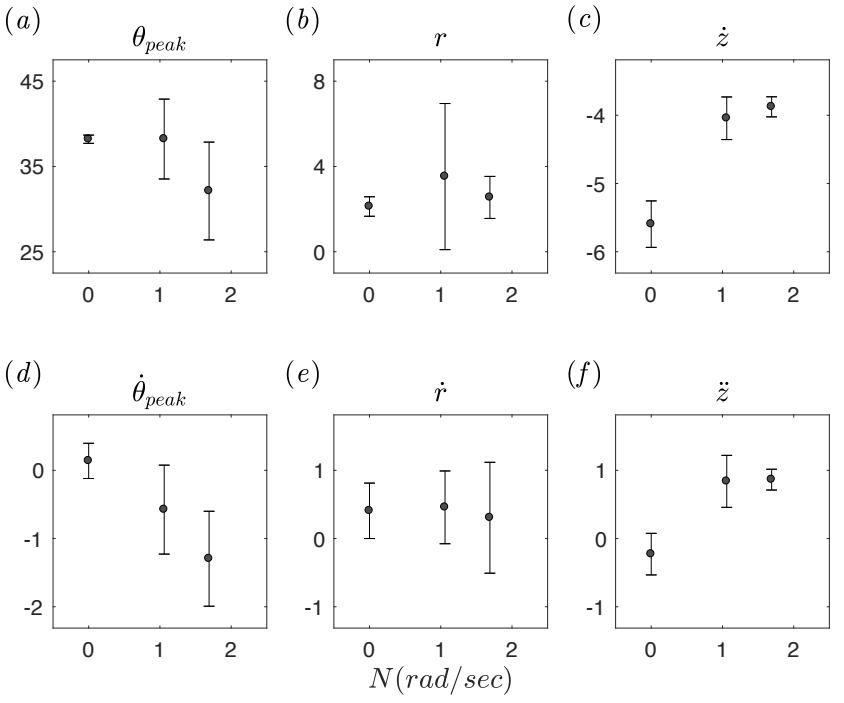

FIGURE 8. Average (a) peak inclination (deg), (b) radial range (cm), (c) vertical speed (cm/sec), (d) peak inclination rate (deg/sec), (e) radial range rate (mm/sec), (f) vertical acceleration (mm/sec^2), for reconstructed descents in pure water ($N = 0$), $N = 1.07\ rad/sec$ and $N = 1.69\ rad/sec$ salt-stratified flow. Error bars are 1σ standard deviations of the mean values from ten reconstructed cases. In (a), larger average peak θ variations are observed for the stratified cases. In (d), non-zero rates in the average peak θ existing, which indicates a reduction in θ as function of time or descent depth. In (f), a positive upward acceleration is observed for stratified flows.

N	θ_{peak}	$\dot{\theta}_{peak}$	r	$\dot{r}$	$\dot{z}$	$\ddot{z}$
(deg/sec)	(deg)	(deg/sec)	(cm)	(mm/sec)	(cm/sec)	(mm/sec^2)
0 (water)	37.9±0.9	0.25±0.33	2.12±2.12	0.41±0.39	–5.60±0.34	-0.23±0.31
1.07	38.2±4.7	-0.58±0.65	3.53±3.43	0.46±0.54	–4.04±0.31	0.84±0.39
1.69	32.1±5.7	-1.30±0.70	2.55±0.99	0.30±0.81	–3.88±0.15	0.85±0.16

TABLE 2. Average reconstructed results for fluttering descents in pure water and salt-stratified flow. Errors are 1σ standard deviations of the mean values from ten reconstructed cases. Results are also summarized in figure 8.

summarized in figure 8 and table 2, including the results from the $N = 1.07\ rad/sec$ stratified flow cases.

4. Discussion

Descent motion of discs and cards have warranted a lot of attention in the recent decades, both experimentally and numerically (see, for example, Ern *et al.* (2012) and

Kuznetsov (2015)). The motion of these free falling objects are generally complex as the solid body and the fluid interacts affecting the path of the falling object. However, for small thickness-to-width ratio the general descent behavior (steady, fluttering, tumbling, or chaotic) can be determined based on the Reynolds number, Re, and the dimensionless moment of inertia, I^* (see Field *et al.* (1997)).

This paper investigated the affect vertical stratification has on the fluttering falling motion of discs. By dropping multiple discs with similar initial conditions and reconstructing their states, we found that stratification enhances the radial dispersion of the disc ($\sigma_{N=1.69}/\sigma_{N=0} \approx 2$), while simultaneously, decreasing the vertical descent speed and the inclination angle during the descent. We note, that wider landing dispersions is usually associated with chaotic descent motion (a combination of fluttering and tumbling) in homogenous fluids, as shown in Heisinger *et al.* (2014). However, stratification appears to perform similar, albeit smaller, enhancing of the absolute radial motion without tumbling, thus, the discs never flips.

The understanding of disc distribution due to stratification effects may have a significant impact on the understanding of unpowered robotic descents, and geological and biological transport, where density and temperature variations may occur. We can imagine engineering applications where such behavior could be useful, for example, placement of photonic solar cells on micro robotics where landing distribution is to be maximized (see Valdes *et al.* 2012; Pounds *et al.* 2016), or enhance our understanding of accidental drops of objects such as pipes during offshore operations (see Yasseri 2014; Majed *et al.* 2013; Awotahegn *et al.* 2016).

Acknowledgements

This work is partially supported by the NSF grant CMMI 13-63404. The authors would like to also thank Stephen Rolfe and Joe Frigo for their assistances with the experiments.

Appendix A

The restoring angular acceleration due to buoyancy for a hydrostatic model is found by first computing the buoyancy offset due to the stratification by integrating the buoyancy element over the disc's volume, then

$$x_B = \frac{\int_V x\rho \; \partial V}{\rho_0 V} \tag{A 1}$$

where $\rho = \rho_0 - |\gamma| x \sin(\theta)$, γ linear fluid density gradient, ρ_0 is the fluid density at the center of the disc, x is the direction along the line of the buoyancy offset centered at the disc, and θ is the inclination angle between the disc's plane and the horizontal plane. In the body centered coordinate system, z is the axis of rotation of the disc, and y normal to the disc plain and completing the right-hand rule. Assuming a cylindrical disc of thickness t and diameter D, the integration yields

$$x_B = -\frac{|\gamma| D^2}{16\rho_0} \sin(\theta). \tag{A 2}$$

The torque due to the buoyancy offset for a pure inclination rotation is then

$$\tau_B = \rho_0 g V x_B \cos(\theta)$$

$$= -\frac{1}{16} gVD^2|\gamma| \sin(\theta)\cos(\theta). \tag{A 3}$$

Similarly, the angular acceleration due to buoyancy for a pure inclination rotation for a homogenous solid disc of density rho_{disc} is found to be

$$\begin{aligned} \ddot{\theta}_B &= -\frac{\rho_0 N^2 V D^2}{16I} \sin(\theta)\cos(\theta) \\ &= -\frac{\rho_0}{2\rho} N^2 sin\,(2\theta) \end{aligned} \tag{A 4}$$

where ρ_0 is the density of the fluid at the disc's center, ρ is the density of the disc, N is the Brunt-Väisälä frequency, and θ is the inclination or nutation angle.

REFERENCES

Andersen, Anders, Pesavento, Umberto & Wang, Z Jane 2005*a* Analysis of transitions between fluttering, tumbling and steady descent of falling cards. *Journal of Fluid Mechanics* **541**, 91–104.

Andersen, A, Pesavento, U & Wang, Z Jane 2005*b* Unsteady aerodynamics of fluttering and tumbling plates. *Journal of Fluid Mechanics* **541**, 65–90.

Auguste, Franck, Magnaudet, Jacques & Fabre, David 2013 Falling styles of disks. *Journal of Fluid Mechanics* **719**, 388–405.

Awotahegn, Michael Berhe, Oosterkamp, Ljiljana Djapic, Nystrøm, Per Richard & others 2016 3d study of dropped object motion in sea water based on scale test. In *The 26th International Ocean and Polar Engineering Conference*. International Society of Offshore and Polar Engineers.

Belmonte, Andrew, Eisenberg, Hagai & Moses, Elisha 1998 From flutter to tumble: inertial drag and froude similarity in falling paper. *Physical Review Letters* **81** (2), 345.

Chrust, Marcin, Bouchet, Gilles & Duek, Jan 2013 Numerical simulation of the dynamics of freely falling discs. *Physics of Fluids* **25** (4).

Ern, Patricia, Risso, Frédéric, Fabre, David & Magnaudet, Jacques 2012 Wake-induced oscillatory paths of bodies freely rising or falling in fluids. *Annual Review of Fluid Mechanics* **44**, 97–121.

Field, Stuart B, Klaus, M, Moore, MG & Nori, Franco 1997 Chaotic dynamics of falling disks. *Nature* **388** (6639), 252–254.

Fortuin, JMH 1960 Theory and application of two supplementary methods of constructing density gradient columns. *Journal of Polymer Science* **44** (144), 505–515.

Heisinger, Luke, Newton, Paul & Kanso, Eva 2014 Coins falling in water. *Journal of Fluid Mechanics* **742**, 243–253.

Hill, DF 2002 General density gradients in general domains: the two-tank method revisited. *Experiments in fluids* **32** (4), 434–440.

Ivey, GN 2004 Stratification and mixing in sea straits. *Deep Sea Research Part II: Topical Studies in Oceanography* **51** (4), 441–453.

Jin, Changqiu & Xu, Kun 2008 Numerical study of the unsteady aerodynamics of freely falling plates. *Comm. Comp. Phys* **3**, 834–851.

Kuznetsov, Sergey P 2015 Plate falling in a fluid: Regular and chaotic dynamics of finite-dimensional models. *Regular and Chaotic Dynamics* **20** (3), 345–382.

Lee, Cunbiao, Su, Zhuang, Zhong, Hongjie, Chen, Shiyi, Zhou, Mingde & Wu, Jiezhi 2013 Experimental investigation of freely falling thin disks. part 2. transition of three-dimensional motion from zigzag to spiral. *Journal of Fluid Mechanics* **732**, 77–104.

MacIntyre, Sally, Romero, José R, Silsbe, Gregory M & Emery, Brian M 2014 Stratification and horizontal exchange in lake victoria, east africa. *Limnology and Oceanography* **59** (6), 1805–1838.

Majed, Arya, Cooper, Phil & others 2013 High fidelity sink trajectory nonlinear simulations

for dropped subsea objects. In *The Twenty-third International Offshore and Polar Engineering Conference*. International Society of Offshore and Polar Engineers.

Maxwell, James Clerk 1990 *The Scientific Letters and Papers of James Clerk Maxwell: 1846-1862*. CUP Archive.

Oster, Gerald 1965 Density gradients. *Scientific American* **213**, 70–76.

Pesavento, Umberto & Wang, Z Jane 2004 Falling paper: Navier-stokes solutions, model of fluid forces, and center of mass elevation. *Physical review letters* **93** (14), 144501.

Pounds, Paul, Potie, Timothy, Kendoul, Farid, Singh, Surya, Jurdak, Raja & Roberts, Jonathan 2016 Automatic distribution of disposable self-deploying sensor modules. In *Experimental Robotics*, pp. 535–543. Springer.

Stringham, GE, Simons, Daryl B & Guy, Harold P 1969 *The behavior of large particles falling in quiescent liquids*. US Government Printing Office.

Tanabe, Yoshihiro & Kaneko, Kunihiko 1994 Behavior of a falling paper. *Physical Review Letters* **73** (10), 1372.

Torres, CR, Hanazaki, H, Ochoa, J, Castillo, J & Van Woert, M 2000 Flow past a sphere moving vertically in a stratified diffusive fluid. *Journal of Fluid Mechanics* **417**, 211–236.

Valdes, Samuel, Urza, Ignacio, Pounds, Paul & Singh, Surya 2012 Samara: low-cost deployment for environmental sensing using passive autorotation. In *Robotics: Science and Systems Workshop on Robotics for Environmental Monitoring*. Citeseer.

Vincent, Lionel, Shambaugh, W Scott & Kanso, Eva 2016 Holes stabilize freely falling coins. *Journal of Fluid Mechanics* **801**, 250–259.

Willmarth, William W, Hawk, Norman E & Harvey, Robert L 1964 Steady and unsteady motions and wakes of freely falling disks .

Yasseri, Sirous 2014 Experiment of free-falling cylinders in water. *Underwater Technology* **32** (3), 177–191.

Yick, King Yeung, Torres, Carlos R, Peacock, Thomas & Stocker, Roman 2009 Enhanced drag of a sphere settling in a stratified fluid at small reynolds numbers. *Journal of Fluid mechanics* **632**, 49–68.

Zhong, Hongjie, Lee, Cunbiao, Su, Zhuang, Chen, Shiyi, Zhou, Mingde & Wu, Jiezhi 2013 Experimental investigation of freely falling thin disks. part 1. the flow structures and reynolds number effects on the zigzag motion. *Journal of Fluid Mechanics* **716**, 228–250.